Received: 28 October 2022 | Revised: 16 March 2023 | Accepted: 27 April 2023

DOI: 10.1002/eqe.3911

SPECIAL ISSUE ARTICLE

WILEY

Evaluation of typology-specific fragility curves used for risk-targeted seismic demand maps in regions of low seismicity: A German case-study

Nicholas Clemett[1] | **Clarissa Rapps**[2] | **Max Gündel**[1]

[1]Chair of steel construction, Helmut-Schmidt-Universität/Universität der Bundeswehr Hamburg, Hamburg, Germany

[2]Wölfel Engineering GmbH + Co. KG, Höchberg, Germany

Correspondence
Nicholas Clemett, Helmut-Schmidt-Universität/Universität der Bundeswehr Hamburg, Hamburg, Germany. Email: nicholas.clemett@hsu-hh.de

Abstract

Investigations of risk targeted peak ground acceleration (PGA) maps for European countries typically adopt a single generic fragility curve definition. The aim of this study is to investigate the use of typology-specific fragility curves in the derivation of risk-targeted PGA maps in low seismicity regions. This study differs from previous works in that it derives expressions for the relationship between design PGA and the median collapse capacity for several different structural typologies designed according to European standards, namely, reinforced concrete (RC) moment-resisting frames (MRFs), reinforced concrete wall and dual systems, and steel MRFs. The expressions were determined from the regression analysis of a database of fragility curve parameters collected from the literature. The influence of the different typology-specific fragility functions on the derivation of risk-targeted seismic maps in regions of low seismicity, using Germany as a case-study, is discussed. The key findings of this study are as follows: the fragility curves derived using the database possess significant inherent lateral capacity; the consideration of this inherent lateral capacity implies the reduction of the regions where seismic design is compulsory; and that fragility curves adapted from fragility analyses from structures in the US may not be representative of European structures. Recommendations for the direction of future research include focusing primarily on improving the definition of the typology-specific fragility curves; developing fragility curves for modern IMs such as average spectral acceleration; and investigating the use of typology-specific curves in regions of high seismicity.

KEYWORDS

Eurocode 8 (EC8), fragility function, risk-targeted demand, seismic design, seismic maps

1 | INTRODUCTION

The derivation of risk-targeted peak ground acceleration (PGA) maps has been a focus of many European studies since the concept was first introduced in the United States (US) by Luco et al.[1] in 2007 and adopted by ASCE 7–10.[2] Unlike the

PRACTITIONER POINTS

- The procedure presented in this paper is consistent with the procedure for simplified reliability-based verification described in Informative Annex E of the draft of the second generation of Eurocode 8.
- Consideration of the failure reliability through typology-specific fragility curves during the initial design phase can lead to lower design peak ground accelerations.
- The use of risk-based seismic demand maps allows designers to target a predefined level of reliability, which is not possible when using hazard-based seismic demand maps.

NOVELTY

- Discusses use of typology-specific fragility functions in the development of risk-targeted seismic demand maps which have not been widely adopted in risk-targeted design studies to date.
- Derives possible relationships between design PGA and median collapse capacity for different structural typologies using data available from the literature. To date the European literature has focused only on reinforced concrete moment frame structures.
- Identifies and discusses key features of typology-specific fragility functions and investigates their influence on risk-targeted design in low seismicity regions in Europe, such as Germany.

hazard-based PGA maps which are used in design codes like Eurocode 8,[3] where the PGAs have a uniform mean annual frequency of exceedance (MAFE), risk-targeted maps display the design PGA required for structures to achieve a desired mean annual rate of failure associated with global collapse (λ_c). The risk-targeted peak-ground acceleration, $a_{g,risk}$, is determined using the equation for λ_c,[4]

$$\lambda_c = \int_0^\infty P\left[F|a_{g,des}, a_g\right] \cdot \left|\frac{dH(a_g)}{da_g}\right| \cdot da_g \tag{1}$$

where $P[F|a_{g,des}, a_g]$ is the probability of failure of a structure designed using a PGA equal to $a_{g,des}$, given the occurrence of a ground motion with a PGA equal to a_g; $H(a_g)$ is the site-specific seismic hazard curve obtained from a probabilistic seismic hazard analysis and represents the MAFE of a PGA intensity equal to a_g. A failure is considered to have occurred when the structure exceeds the collapse limit state and $P[F|a_{g,des}, a_g]$ can be thought of as the collapse fragility curve, as it is referred to from hereon, which represents the distribution of the collapse capacity of the structure. $a_{g,risk}$ can be calculated iteratively with Equation (1) until λ_c equals, within an acceptable tolerance, a target value, $\lambda_{c,t}$. For each iteration, a trial value of $a_{g,des}$ is selected. This value is used to define an appropriate collapse fragility curve and determine the corresponding λ_c. If λ_c is greater than $\lambda_{c,t}$, it indicates that a structure designed with the trial value of $a_{g,des}$ has insufficient capacity to meet the target reliability level and $a_{g,des}$ needs to be increased. The opposite is true if λ_c is less than $\lambda_{c,t}$. This procedure is repeated until an $a_{g,des}$ is found such that $\lambda_c \cong \lambda_{c,t}$. The final value of $a_{g,des}$ is then adopted as $a_{g,risk}$.

A significant advantage of using a risk-targeted method to determine the design PGA is that it incorporates both the uncertainty of the collapse capacity of the structure and the complete hazard curve into the calculation. This results in a more robust and less arbitrary estimate of the reference PGA (compared to a purely hazard-based approach) which targets a uniform and predefined level of seismic reliability. Apart from the in US, maps of $a_{g,risk}$ have been developed for European countries such as France,[5] Italy,[6,7] Romania,[8] Spain,[9] as well as Europe as a whole,[10] Iran,[11,12] Brazil,[13] and New Zealand.[14]

An important part of the derivation of $a_{g,risk}$ is the fragility curve that is used to represent the uncertainty in the collapse capacity of the structures. In the seminal US study, the structural capacity was modeled as a log-normal random variable defined by

$$P\left[C|a_{g,des}, a_g\right] = \Phi\left(\frac{\ln(a_g) - \ln(a_{g,des}) - \Phi^{-1}(P[C|\, a_g = a_{g,des}\,])\cdot\beta_c}{\beta_c}\right) \tag{2}$$

with a dispersion, $\beta_c = 0.8$, and a probability of collapse conditioned on $a_{g,des}$, $P[C|\, a_g = a_{g,des}\,]$, of 10% .[1] In Equation (2), F has been replaced with C to explicitly indicate that failure is the collapse of the structure. In the US, $a_{g,des}$ corresponds to the Maximum Considered Earthquake generally defined as having a return period (RTP) of 2475 years. These values for β_c and $P[C|a_{g,des}]$ were originally selected based on the results of dynamic nonlinear time-history analyses of structures conforming to the NEHRP 2003 seismic design provisions which were performed as a part of the ATC-63 project to develop FEMA P695 guidelines.[1,15]

The fragility curve used by Luco et al.[1] has strongly influenced the subsequent European studies, with several adopting the values for β_c and $P[C|a_{g,des}]$ directly[8] or modifying $P[C|a_{g,des}]$ to be representative for design ground motions corresponding to RTPs other than 2475 years.[6] In their study of $a_{g,risk}$ for France, Douglas et al.[5] adopted $\beta = 0.5$ and $P\,[C|a_{g,des}] = 1 \cdot 10^{-5}$ (for a 475-year design ground motion) following a sensitivity analysis and based on the fact that, when paired with a suitable $\lambda_{c,t}$, the chosen values did not result in significant changes to the existing level seismic demand. Silva et al.[10] selected $\beta = 0.6$ after performing a statistical analysis of fragility curves for European reinforced concrete (RC) moment-resisting frames (MRFs) and accounting for some additional level of uncertainty. In the same study $P\,[C|a_{g,des}] = 1 \cdot 10^{-3}$ was adopted after inspecting the results of detailed collapse assessment studies from the US and modifying $P[C|a_{g,des}]$ for a 475-year RTP.

To help improve the calculation of $a_{g,risk}$, Martins et al.[16] conducted an extensive investigation of the collapse fragility of regular European RC MRFs and developed relationships for the median collapse PGA, θ_c, and β_c as a function of $a_{g,des}$. When defining the fragility curve in terms of the median collapse capacity, Equation (2) can be replaced with

$$P\left[C|a_{g,des}, a_g\right] = \Phi\left(\frac{\ln(a_g) - \ln(\theta_c(a_{g,des}))}{\beta_c(a_{g,des})}\right) \tag{3}$$

A significant advantage of these relationships over the fragility curves described in the previous paragraph is that the definition of the hazard curve is no longer dependent on an assumption for $P[C|\, a_g = a_{g,des}]$; the values of which can vary significantly as highlighted by previous studies.[10] Additionally, this new definition of the fragility curve also removes the assumption that $a_{g,des}$ and θ_c are directly proportional, as implied by Equation (2). The fragility curves proposed by Martins et al.[16] adopted by Crowley et al.[17] for their study on risk targeted ground motions considering individual and societal risk. Kharazian et al.[9] used a multivariate distribution of β_c and $P[C|a_{g,des}]$, derived from the work of Martins et al.,[16] to determine the characteristics of the mean fragility curve and the statistical variation of β_c and $P[C|a_{g,des}]$ so that a sensitivity analysis could be conducted for $a_{g,risk}$ maps for Spain.

From the brief review highlighted in the preceding paragraphs several conclusions can be drawn: First, most studies in the literature either directly adopted one or more of the fragility parameters proposed by Luco et al.,[1] or use them in conjunction with the results from other US studies to estimate new values; second, when European data is used to derive suitable parameters for the fragility functions, the data is exclusively from studies considering RC MRFs. Although RC MRFs constitute a significant portion of the European building stock, it is not necessarily acceptable to assume that the other structural typologies, such as RC wall and dual systems (RC-WDSs) or steel MRFs (S-MRFs) exhibit the same fragility characteristics. This is an important point to note, particularly if the goal is to achieve the desired reliability target on a building-by-building basis.

This paper presents a preliminary investigation into typology-specific fragility functions for European RC-MRFs, RC-WDSs and S-MRFs for use in deriving risk-targeted seismic demand maps for Europe. Expressions for θ_c and β_c are developed by performing regression analysis on a database of fragility curves gathered from the literature. These expressions are then compared to the existing literature and the differences discussed. The influence of the typology-specific fragility curves on the derivation of $a_{g,risk}$ maps for regions of low seismicity are then discussed, using the case of Germany as an example. Finally, recommendations for future work are proposed.

2 | FRAGILITY FUNCTIONS OF BUILDINGS DESIGNED ACCORDING TO EUROCODE 8

2.1 | Literature review of available fragility curves

To evaluate the fragility curves available for the derivation of typology-specific seismic demand maps, a literature review was conducted, and fragilities curves were collected from a range of different studies. A summary of the studies which yielded suitable fragility curves is presented in Table 1.

TABLE 1 Summary of the fragility curves gathered from the literature

	Structural system	Ductility classes	# stories	Analysis method	Intensity measure
Concrete structures					
Pitilakis et al.[18]	MRF, W, D	n/g	1–3, 4–7, 8+	SPO	PGA
Ulrich et al.[19]	MRF	M	3	Cloud	PGA
Saruddin and Nazri[20]	MRF	M	3, 6	IDA	PGA
Nazri et al.[21]	MRF	M	3, 6, 9	IDA	PGA
Gkimprixis et al.[22]	MRF	M	2, 4	IDA	PGA
Martins et al.[16]	MRF	M	3, 5	MSA	PGA
Lazar and Dolšek[23]	MRF	M, H	4, 6, 8, 11, 15	IDA	PGA
Žižmond and Dolšek[24]	MRF	n/g	8, 11	IDA	PGA
Kosič et al.[25]	MRF, W	M	2, 4, 5, 6, 8	IDA	SA(T1)
Aljawhari et al.[26]	MRF	H	4	Cloud	AvgSA
Steel/composite structures					
Braconi et al.[27]	MRF	M	5	IDA	PGA
Nazri et al.[21]	MRF	M	3, 6, 9	IDA	PGA
Saruddin et al.[20]	MRF	M	4, 5, 6	IDA	PGA
Macedo et al.[28]	MRF	M, H	2, 3, 4, 5, 8	IDA	SA(T1)
Tartaglia et al.[29]	MRF	n/g	3, 6	IDA	SA(T1)

Abbreviations: AvgSA, average spectral acceleration; Cloud, cloud analysis; D, dual wall-frame systems; H, high; IDA, incremental dynamic analysis; M, medium; MRF, moment-resisting frames; MSA, multiple-stripe analysis; n/g, information not given; PGA, peak ground acceleration; SA(T1), spectral acceleration at the first mode period; SPO, static pushover; W, walls.

For a fragility curve to be considered suitable for inclusion in the database used in this study it must fulfill several criteria. First, the structure, which the fragility curve represents, must be designed in accordance with the framework of the Eurocode standards, including not just the seismic provisions of Eurocode 8[3] but also the material-specific standards, such as Eurocode 2[30] for RC structures and Eurocode 3[31] for steel structures. These structures can be considered typical of new buildings designed in European countries such as France, Italy, and Germany, amongst others. Fragility curves derived for old pre-code structures were not considered in this study. Second, enough information must be provided to be able to determine the design PGA or design spectral acceleration (SA) of the structure. During this review, it became evident that this was not always the case and several studies that were reviewed, for example,[32–34] were not able to be included because the design level acceleration was not clear or could not be back calculated from the available information. Third, the fragility curves need to represent the global collapse limit state of the structure, because $a_{g,risk}$ is defined as the design PGA that results in the target mean annual frequency of collapse. There are several studies in the literature[35–38] that produce numerous fragility curves for the life-safety or significant damage limit-states however, these limit-states do not describe collapse and were subsequently excluded from this study. It is acknowledged that there are ratios that could have been used to estimate the probability of collapse given the occurrence of these lesser damage states (e.g., from HAZUS[39]). However, due to the epistemic uncertainty involved in deriving these ratios and the fact that they have been derived for structures in the United States, they were not included in this study.

The intensity measure (IM) used to condition the fragility curve is also an important consideration. Three different scalar IMs have been included in the literature review: PGA; SA at the first mode period, SA(T1); and the average SA (AvgSa). A short discussion regarding the different IMs is presented in the following section.

2.2 | Selection of the conditioning IM

The background information and review of past studies presented in §1 uses the PGA as the conditioning IM for the fragility function. This is, of course, not the only option and fragility curves for new Eurocode-8-conforming structures have also been derived for SA(T1) and AvgSa IMs (refer to Table 1). Any of these IMs could be used in lieu of the PGA in the risk-targeted procedure described previously, each having its own advantages and disadvantages. In this study, PGA was selected as the IM for the fragility curves because it is the IM that is used to anchor the design response spectrum currently adopted in Eurocode 8 and it is familiar to both practicing engineers and researchers. It is acknowledged that

the new draft of Eurocode 8 is proposing the use of a response spectrum that is, anchored by two SA ordinates, replacing the single PGA value. Either of these spectral ordinates, S_α, the maximum response SA (i.e., the plateau value), or S_β, the SA at a period of 1 s, or even a spectral ordinate at another period could be used to condition the fragility curves. However, most of the SA(T1) fragility curves are conditioned on the SA periods that do not necessarily correspond to either S_α or S_β (e.g., SA(T1 = 0.6s) or SA(T1 = 1.5s)). This means, in order to have a large enough data set to investigate the relationship between the median failure capacity and the design acceleration, the fragility curves would need to be harmonized in terms of the conditioning IM. Choosing PGA as the conditioning IM requires the least number of fragility curves to be modified, helping to minimize the increase in the dispersion of the median capacities resulting from the conversion.

Another attractive feature of PGA is that it is an IM that is, independent of the properties of the structure, making it convenient for the development of typology-specific seismic demand maps. A significant drawback, however, is that it is not a very efficient IM and is not very well correlated with structural damage. Using SA(T1), which is a more efficient IM than PGA,[40] could alleviate this issue. However, this would require the development of several maps for each structural typology (i.e., one for each period of interest) making their practical implementation in design codes cumbersome and potentially confusing. An attractive alternative to PGA and SA(T1) is AvgSa. Like PGA, AvgSa could be used to create a single seismic demand map for each typology, whilst offering significant improvements in the prediction of the structural response.[40,41] Unfortunately, as it is a relatively modern IM, there have been relatively few studies in the literature where significant numbers of fragility curves for new Eurocode-8-conforming structures have been produced, which makes it impractical for use in this study.

2.3 | Conversion of fragility curve IMs

As mentioned in the previous section, harmonization of the fragility curves in terms of the conditioning IM is required if all the data points are to be used for the statistical analysis. Hazard-consistent procedures for converting fragility curves between different IMs exist, for example, Suzuki and Iervolino,[42] however these are site-specific and require disaggregation of the site-hazard, which was not considered feasible for a study at the regional level. A simpler, albeit more approximate, approach is to use the typical shape of the Eurocode 8 response spectrum to move from one spectral ordinate to another. By converting the fragility curves from one IM to another, additional dispersion of the median collapse capacities will likely to be introduced when the entire database is considered. To monitor the impact that using the converted fragility curves will have on the relationship between the design acceleration and the failure capacity, comparisons are made between the complete database (including the converted values) and the unconverted values, where applicable.

2.4 | The fragility database

Based on the discussion in the previous section it was decided that the initial database would consist of all the fragility curves using PGA and SA(T1) as the conditioning IM. The SA(T1)-based fragility curves were converted to PGA using the response spectrum procedure briefly described in §2.3. The fragility curves using AvgSa was not considered in this study as there are only a small number relative to the other IMs, and they could not be converted to PGA in such an easy manner. A summary of all the median collapse capacities (in terms of PGA) of the fragilities collected in this study is presented in Figure 1. Fragility curves originally conditioned on SA(T1) are indicated with crosses, while those conditioned on PGA are shown by circles.

A total of 136 fragility curves were obtained for RC MRFs and 21 for RC WDS. It is not surprising that most studies concerned RC MRFs, given their prevalence in the European building stock. All the concrete structures were designed using the Type 1 acceleration response spectrum from Eurocode 8[3] and $a_{g,des}$ ranged between 0 $m{\cdot}s^{-2}$ and 5 $m{\cdot}s^{-2}$. Generally, the MRFs have been designed in accordance with the provisions for ductility class "Medium", although in some cases ductility class "High" was used or the information was not provided.[18]

From Figure 1, unlike RC MRF structures, the literature does not provide a significant amount of data related to the collapse fragility curves of RC WDS. There are several studies that investigated the fragility of WDS structures in a European context[35,38] and produced many analytical fragility curves; however, they described the fragility of the ultimate limit state and not collapse. The wall and dual system fragility data in the database comes from just two studies, one using PGA as the IM[18] and the second SA(T1).[25] Although not ideal, it still serves the purpose of this study, which is to illustrate why it is important to consider typology-specific fragility curves. This is evidenced in Figure 1, where θ_c is significantly higher for the MRFs than the WDSs for the same $a_{g,des}$.

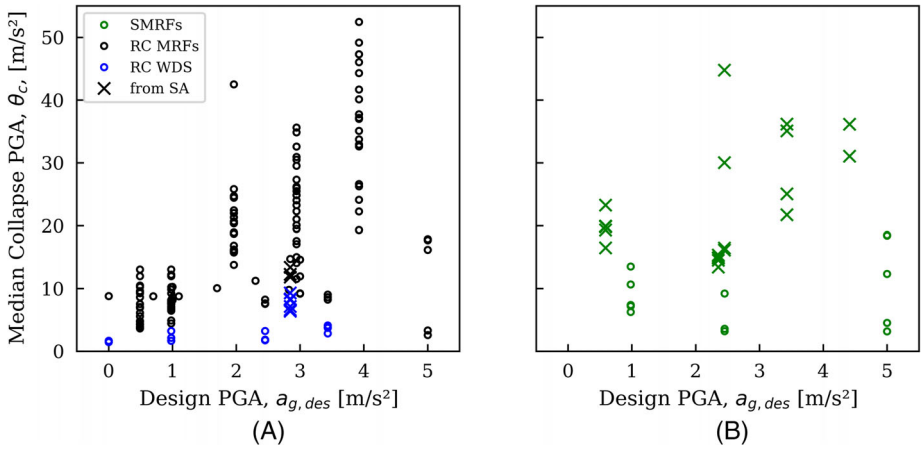

FIGURE 1 Median collapse capacity, θ_c, of fragilities curves in the database. (A) RC frame, wall, and dual systems. (B) Steel and composite moment-resisting-frame systems. Circles indicate fragility curves that use PGA as the original IM and crosses correspond to fragility curves with an original IM of SA(T1). IM, intensity measure; PGA, peak ground acceleration; RC, reinforced concrete; SA(T1); SA at the first mode period.

It also proved difficult to find suitable fragility curves for steel MRFs and braced frames in the literature, as evidenced by the small number of data points in Figure 1B. A total of 33 fragilities for steel and steel composite MRF structures were obtained from the literature. Both Type 1 and 2 design spectra were used for the design of these structures, and $a_{g,des}$ varied between 0.5 m·s^{-2} and 5 m·s^{-2}. Figure 1B shows the plot of θ_c for each fragility curve in the database against the corresponding $a_{g,des}$. It is worth noting that the median collapse capacities of the structures originally conditioned on SA(T1) are much higher than those conditioned on PGA.

A feature of the relationship between the θ_c and $a_{g,des}$ that can be seen in Figure 1A, is that θ_c tends to approach a constant value for smaller values of $a_{g,des}$. This observation has been noted in prior studies on this topic[19] and can be attributed to the fact that, for low values of $a_{g,des}$, the gravity load design, wind loading, and minimum geometric or cross-sectional design requirements, all of which are independent of $a_{g,des}$, can govern the lateral resistance of the structure.[16,43]

The characteristics of the dynamic analyses, such as the number of records, the record selection, and the procedure used to fit the fragility curves can also have a significant influence on the quality of the results and the subsequent derivation of the fragility curves. There is a significant variation in the number of records used for the IDA across the studies. Most studies use 14 or more records[22,23,25,28,29] which tends to be in line with typical engineering practice, however some studies use only seven[20] or even three,[21] citing the fact that, at the time the studies were produced, this was the code mandated minimum requirement. The effect of the reduced number of records appears to be evident in the results, with both studies[20,21] tending to exhibit lower median collapse and dispersion values than the rest of the studies on RC structures. The study by Martins et al.[16] was very thorough and selected 30 records for each stripe of the MSA. The methods used to select the records varied across the studies. Several studies did not use hazard consistent ground motion selection procedures but rather selected ground motions from databases like the NGA database or the European Strong Motion Database such that the median matched the target spectra, which could either be a site-specific spectrum[23] or the Eurocode 8 design spectrum.[25,29] Other studies considered a more scenario-based approach, where a series of criteria were set based on magnitude and source-to-site distance and suitable records were extracted from the database.[22] Finally, Martins et al.[16] performed a hazard consistent record selection and scaled the records using a modified version of the conditional spectrum method.

2.5 | RC fragility curves

2.5.1 | Median collapse capacity

As noted in the previous section, there is a clear difference between θ_c for RC MRFs and the RC WDS. For this reason, RC MRFs and RC WDS will be considered separately.

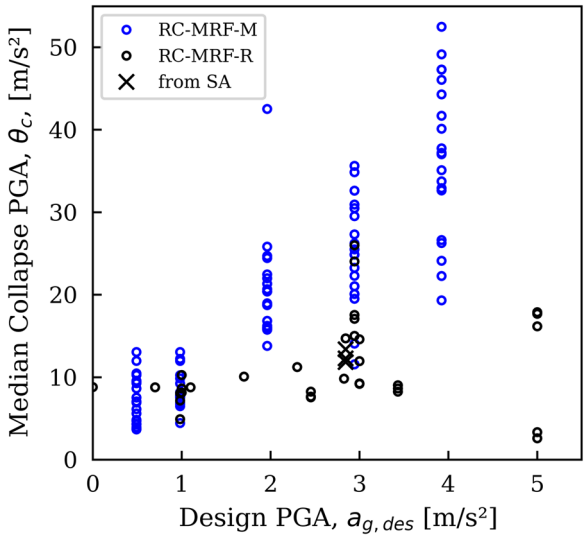

FIGURE 2 Median failure PGAs of the fragility curves for RC MRFs. Circles indicate fragility curves that use PGA as the original IM and crosses correspond to fragility curves with an original IM of SA(T1). IM, intensity measure; MRFs, moment-resisting frames; PGA, peak ground acceleration; RC, reinforced concrete; SA(T1); SA at the first mode period.

Recently, Martins et al.[16] conducted a study focused on developing fragility curves of new RC MRFs designed according to Eurocode 8 for use in the development of $a_{g,risk}$ maps. In this study, a suite of three-dimensional three and five-story regular RC MRF buildings with variable beam span and story height were designed for $a_{g,des}$ values of 0.05 , 0.1 , 0.2 , 0.3 , and 0.4 g. Subsequently, the collapse fragility curve for each building was determined from the results of a Multiple Stripe Analysis (MSA). The detailed work of Martins et al.[16] contributes 100 of the 136 fragility curves that comprise the RC MRF database. The remaining 36 fragility curves come from eight other studies. As evidenced in Table 1, most of the studies use nonlinear dynamic analysis methods such as Cloud analysis, or Incremental Dynamic Analysis (IDA) to determine the fragility curves.[16,19–25] Static analysis methods (SPOs), such as the pushover-over analysis, have also been used to estimate the median performance points of some structures and were coupled with assumed values of the coefficient of variation to estimate the dispersion of the corresponding fragility curves.[18] The buildings in the database are generally, low-midrise structures varying between two and nine stories tall, depending on the study considered, with several up to 11 and 15 stories tall.

Figure 2 shows a comparison between θ_c of the fragility curves from the study of Martins et al.[16] (RC-MRF-M) and those from the remaining studies[18–25] (RC-MRF-R). It is evident that there is a significant difference in the values of θ_c between the two groups, which could possibly be related to the maximum drift limits and the definition of the collapse point of the structures in the studies or the analysis method. Given the large differences observed, the fragility curves from Martins et al.[16] cannot be used in conjunction with the remaining. From this point on, two sets of RC MRF fragility data will be considered; RC-MRF-M, comprising the fragility curves of Martins et al.[16]; and RC-MRF-R which encompasses the data from the remaining studies.

To determine if θ_c is dependent on parameters other than $a_{g,des}$, the MRF fragility curve database was disaggregated and critically analyzed. The results of the disaggregation are presented in Figures 3 and 4 for the RC-MRF-R and RC-MRF-M datasets, respectively. Figure 3A presents the disaggregation of the database according to the number of stories of each building. There appears to be significant overlap between the different groups and no clear trend is evident. The disaggregation of the database according to the analysis method used to determine the fragility curves is presented in Figure 3B. The choice of analysis method appears to have an influence on θ_c: studies utilizing nonlinear dynamic analysis techniques such as IDA or cloud analysis consistently produce higher median collapse values, when compared to the SPO.

Contrary to the relationship observed in Figure 3, the five-story buildings in the RC-MRF-M dataset (Figure 4) exhibit higher θ_c than the three-story buildings, with a variation of up to 50% in the mean values. This difference is reasonably significant, yet it is difficult to generalize the relationship given that only three- and five-story structures were analyzed.

In the case of the RC WDS, there is insufficient data to be able to disaggregate the database and draw conclusions about the influence of the analysis methods or the number of stories.

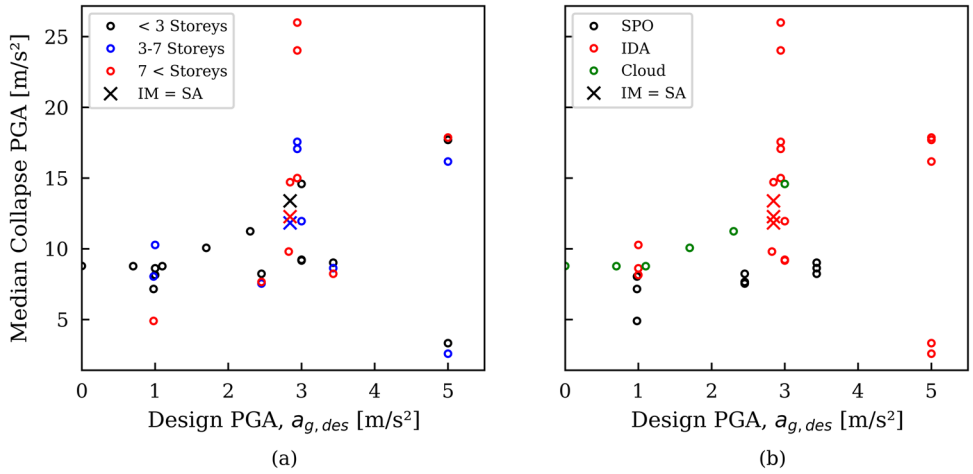

FIGURE 3 Disaggregation of the RC-MRF-R database. (A) The number of stories; (B) Analysis method. Circles indicate fragility curves that use PGA as the original IM and crosses correspond to fragility curves with an original IM of SA(T1). IM, intensity measure; MRFs, moment-resisting frames; RC, reinforced concrete; SA(T1); SA at the first mode period.

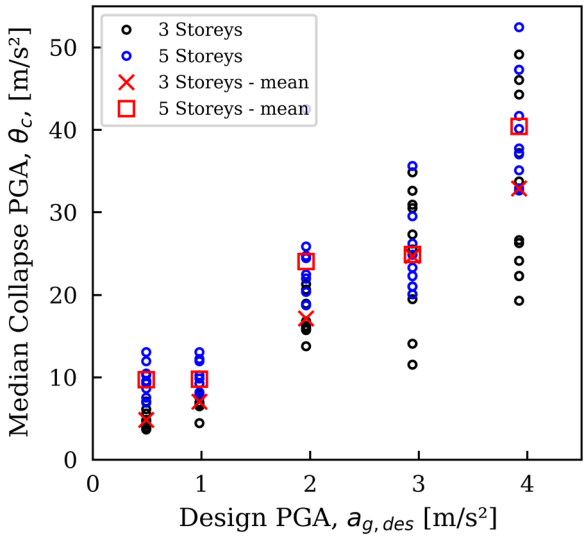

FIGURE 4 Disaggregation of the RC-MRF-M database according to number of stories. The mean values are shown in red. M, medium; MRFs, moment-resisting frames; RC, reinforced concrete.

Based on these observations, it was decided, for this study, that the relationship between θ_c and $a_{g,des}$ could be considered independent of the number of stories and the analysis method for the RC-MRF-M and RC-WDS databases. For the RC-MRF-R database the influence of the analysis method is clear and cannot be ignored. Before an expression for θ_c could be determined, unsuitable fragility curves needed to be removed from the database. In the case of RC-MRF-R, several fragility curves obtained from the study of Saruddin et al.[20] were removed from the database because the values of θ_c were significantly less than $a_{g,des}$. The probability of collapse for the design level acceleration for these curves were 89% and 95%. These values were considered unrealistic when compared to the other values in the database, which typically lie around a 1% probability of collapse at the design level, and, as mentioned in §2.4, can probably be attributed to the low number records used during the structural analysis.

It is worth noting, that several data points in the wall and dual system database also have θ_c less than unity, corresponding to probabilities of collapse of around 80%–95% at the design level. These were also considered unsuitable and removed. Of the remaining data points that the average probability of collapse at the design level was around 15%. The lower capacities and higher probabilities of collapse of the wall and dual systems could possibly be attributed to the use of the more simplified and conservative SPO analysis method to determine the fragility curves.

TABLE 2 Parameters defining the relationships between θ_c, β_c, and $a_{g,des}$ for the fragility curves investigated in this study.

Fragility Curve	Description	m_{θ_c}	c_{θ_c}	m_{β_c}	c_{β_c}	β_{β_c}	Inherent Cap. [m·s^{-2}]
RC-MRF-R	Full database	2.11	6.54	–	–	–	8.09
RC-MRF-R-PGA	only origin IM = PGA	2.11	6.54	–	0.54	0.13	8.09
RC-MRF-R-DYN	Only dynamic analyses	2.17	7.71	–	–	–	8.92
RC-MRF-R-STAT	Only static analyses	0.78	5.92	–	–	–	6.70
RC-MRF-M	Full database	8.58	1.86	0.06	0.57	0.10	7.84
RC-MRF-M-RTO	Regression through origin	9.19	–	0.06	0.57	0.10	–
RC-WDS	Full database	1.31	1.30	–	–	–	1.98
RC-WDS-PGA	only origin IM = PGA	0.51	1.49	–	0.22	0.07	1.98
S-MRF-PGA	only origin IM = PGA	0.73	6.98	–	0.27	0.16	9.00
S-MRF-SA	only origin IM = SA	3.54	14.90	–	–	–	19.77
Douglas et al.[5]	–	8.43[a]	–	–	0.5	–	–
Luco et al.[1]	–	7.46[a,b]	–	–	0.8	–	–

Abbreviations: DYN, dynamic analyses; M, data from Martins et al[16].; MRF, moment-resisting frames; PGA, peak ground acceleration; RC, reinforced concrete; RTO; regression through the origin; S, steel; SA, spectral acceleration; STAT, static analyses; WDS, wall and dual systems.

[a]The m_{θ_c} values for Douglas et al.[5] using $P[C|a_{g,des}] = 1 \cdot 10^{-5}$, $\beta = 0.5$ and Luco et al.[1] using $P[C|a_{g,des}] = 6 \cdot 10^{-3}$, $\beta = 0.8$, where $P[C|a_{g,des}]$ is the probability of collapse for the 475-year design motion.

[b]A suitable value of x for the 475-year RTP was determined following the procedure outlined by Silva et al.,[10] adopting the average value obtained considering all sites in Germany.[45]

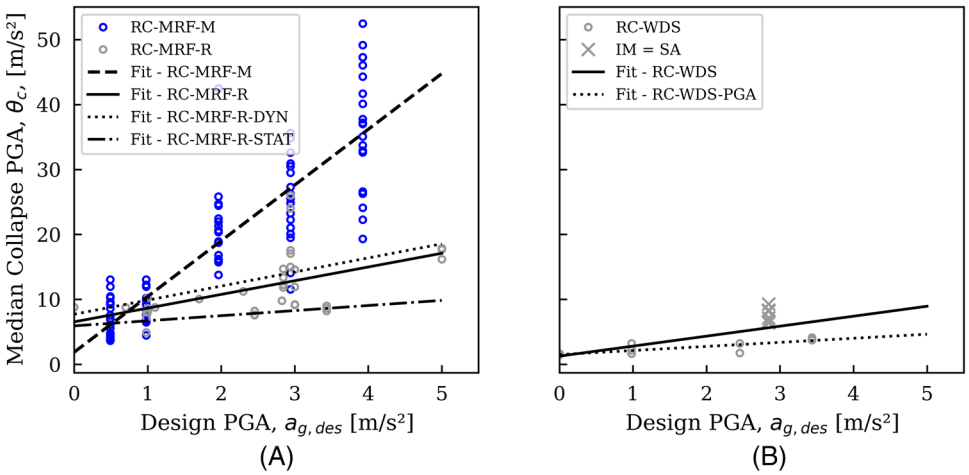

FIGURE 5 The final θ_c databases and the regression lines for (A) the RC-MRF-R and RC-MRF-M data, and (B) the RC-WDS data. M, medium; MRFs, moment-resisting frames; RC, reinforced concrete.

A linear regression was used to model the relationship between θ_c and $a_{g,des}$ for both sets of RC MRFs and the RC WDS. The corresponding equation is given by,

$$\theta_c = m_{\theta_c} \cdot a_{g,des} + c_{\theta_c} \tag{4}$$

The regression was performed using the SciPy statistics module for Python and the results are presented in Table 2. It is worth noting here that a regression of the RC-MRF-M data has already been conducted by Crowley et al.,[17] however, this fit was conducted using the mean values for each PGA level. By repeating the regression analysis using all the data, we can quantify the additional uncertainty resulting from the dispersion about the best fit line. The finalized databases and the corresponding regression lines are presented in Figure 5. As part of the data analysis and a preliminary study,[44] several different regression models were trialed, and the fits compared with each other, during which the linear regression model was seen to perform favorably. For brevity, the results of this analysis are not presented herein but interested readers are

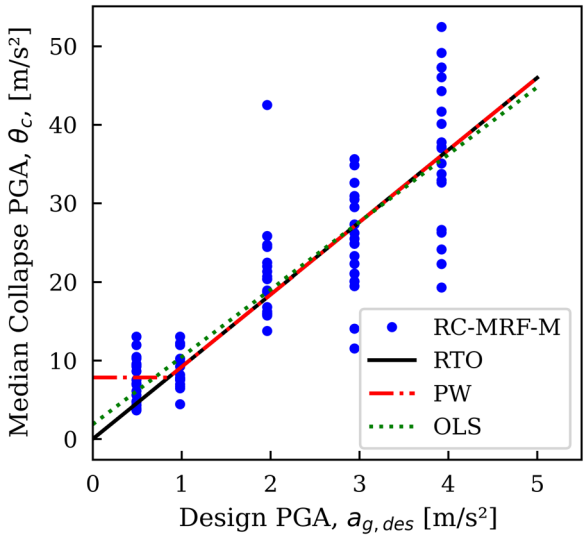

FIGURE 6 Piecewise and RTO model for $\mathbf{a_{g,des} - \theta_c}$ relationship derived for the RC-MRF-M dataset. M, medium; MRFs, moment-resisting frames; RC, reinforced concrete.

referred to the end of this paper where they can find a link to all the data and scripts used in this study and the comparison of the different regression models.

Four different fits have been performed on different portions of the RC-MRF-R database. The first fit, RC-MRF-R considers all the data points shown in Figure 3, including the points derived from fragilities conditioned on SA(T1). The second fit, RC-MRF-R-PGA, considers only the data points which were originally conditioned on PGA. It is clear from the results in Table 2 that there is little deviation when compared to the fit using all the points, although this is most likely due to the fact that the RC-MRF-R database only contains a small number of points converted from SA(T1). The remaining two fits, RC-MRF-R-DYN and RC-MRF-R-STAT are regressions considering only the results determined from dynamic analyses (-DYN) and static analyses (-STAT) respectively.

Two different fits were considered for the RC-WDS database; one utilizing all the data points irrespective of the original conditioning IM (RC-WDS), and a second considering only the values originally conditioned on PGA (RC-WDS-PGA). From Figure 5, the inclusion of the SA(T1) points increases the slope of the θ_c -$a_{g,des}$ relationship markedly.

Fitting a linear regression to the median collapse capacity data, as depicted in Figure 5, results in an equation that yields a non-zero collapse capacity when extrapolated to $a_{g,des}$ equal to zero. As already mentioned in the preceding section, this can be attributed to factors other than the seismic loading. However, considering the RC MRFs, and in particular RC-MRF-M, the inherent capacity is not accurately predicted by extrapolating the linear regression model below $a_{g,des}$ of 1 m·s^{-2}. Figure 5 shows that the lateral capacity of the RC-MRF-M structures tends to plateau when $a_{g,des}$ is less than 1 m·s^{-2}. To better model this inherent lateral capacity, the $a_{g,des} - \theta_c$ relationship for RC-MRF-M was redefined using a piecewise linear model. First, a regression through the origin (RTO) was performed excluding the data for a_g equal to 0.49 m·s^{-2}. The corresponding slope, m_{θ_c} is presented in Table 2. Second, the plateau value was taken as 7.84 m·s^{-2}, which corresponds to the mean lateral capacity for of the RC-MRF-M data set for $a_{g,des}$ less than 1 m·s^2. Last, the value of $a_{g,des}$ at the end of plateau (0.82 m·s^{-2}) is defined by intersection of the plateau and the slope of the RTO. A comparison of the piecewise model (PW) accounting for the inherent lateral capacity, the RTO and the original ordinary least-squares regression (OLS) is presented in Figure 6. The slope determined using RTO can be directly compared to fragility models used in the literature which assume a perfectly linear relationship between θ_c and $a_{g,des}$ (e.g.,[1,5]).

Similar piecewise fits were developed for the remaining models, but without using RTO. Instead, the value of the inherent capacity was intersected with the unconstrained lines of best fit given in Table 2.

2.5.2 | Dispersion of the fragility curves

A large variation in the dispersion of the fragility curves was observed across the reviewed studies, the values which are presented in Figure 7. Only the dispersions of the fragility curves included in the final databases produced in §2.5.1 were

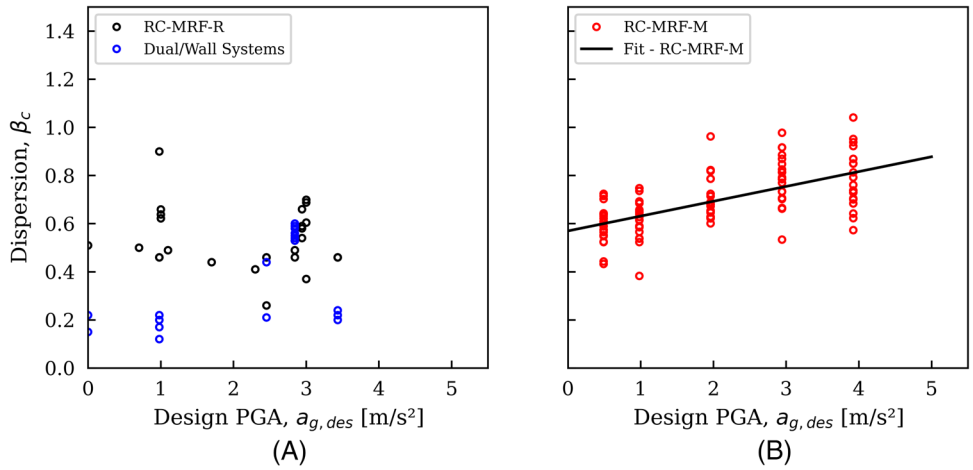

FIGURE 7 This β_c values from the database. (A) Dual walls and RC-MRF-R, (b) RC-MRF-M and corresponding regression. M, medium; MRFs, moment-resisting frames; RC, reinforced concrete.

considered; however, the dispersions from the study of Nazri and Saruddin[21] were excluded because the reported values between 0.02 and 0.05 were unrealistically low for structures designed for an $a_{g,des}$ of 5.0 m·s^{-2}, again, this is most likely due to the fact that only three records were used for the structural analysis. Figure 7 presents the dispersion values of the fragility curves from the databases for both sets of RC MRFs and the RC WDS. Only the dispersions associated the fragility curves originally conditioned on PGA were considered, because the dispersion of the curves originally conditioned on SA(T1) could not be converted to PGA in the same way as the median values. For this reason, Table 2 only shows values for the—PGA fits. These dispersion characteristics were assumed for the related fits of each database.

In Figure 7A, there appears to be a very weak correlation between $a_{g,des}$ and the dispersion. For RC-WDS the trend is positive, while for RC-MRF-R it is negative. A reduction in dispersion with increasing design PGA seems counterintuitive given that structures designed for stronger shaking are likely to exhibit higher levels ductility, during which geometric and nonlinear effects will have a greater influence, thus increasing the variability of the response. Considering this, the observed weak correlation, and the fact that there are only a small number of data points for design PGAs greater than 3.0 m·s^{-2}, a constant dispersion across all design PGAs was assumed for RC-MRF-R and RC-WDS. The adopted values were taken as the mean of the corresponding data points and are presented in Table 2. Unlike RC-MRF-R, the dispersion values from RC-MRF-M showed a distinct positive correlation, which could be modeled using linear regression.[17] The resultant linear model is of the form,

$$\beta_c = m_{\beta_c} \cdot a_{g,des} + c_{\beta_c} \tag{5}$$

where the values of m_{β_c} and c_{β_c} are presented in Table 2.

2.6 | Steel fragility curves

θ_c and β_c from the steel fragility curve database are presented in Figure 8. As highlighted in §2.1 there is a significant difference between the median capacities taken from studies originally conditioned on SA(T1) and those conditioned on PGA; the former being significantly higher. As a result, the steel database was separated into two sub databases; one containing only the converted SA(T1) data points, S-MRF-SA; and the second containing only the data points originally conditioned on PGA, S-MRF-PGA. Like the RC-MRF-R and RC-WDS databases, several points were removed due to unrealistic probabilities of collapse at the design level, specifically, the points from the study of Saruddin and Nazri,[20] which exhibited probabilities of collapse of 60% and 89%.

Given the smaller number of fragility curves available in each of these steel structure databases, conducting a sensitivity analysis, like that for the RC buildings, was not feasible. Instead, the regression was fitted directly to the median collapse capacity data as shown in Figure 8A. The resulting parameter estimates are reported in Table 2. It is acknowledged that the data, specifically the fragilities conditioned on PGA, may not be the truly representative of the behavior steel structures,

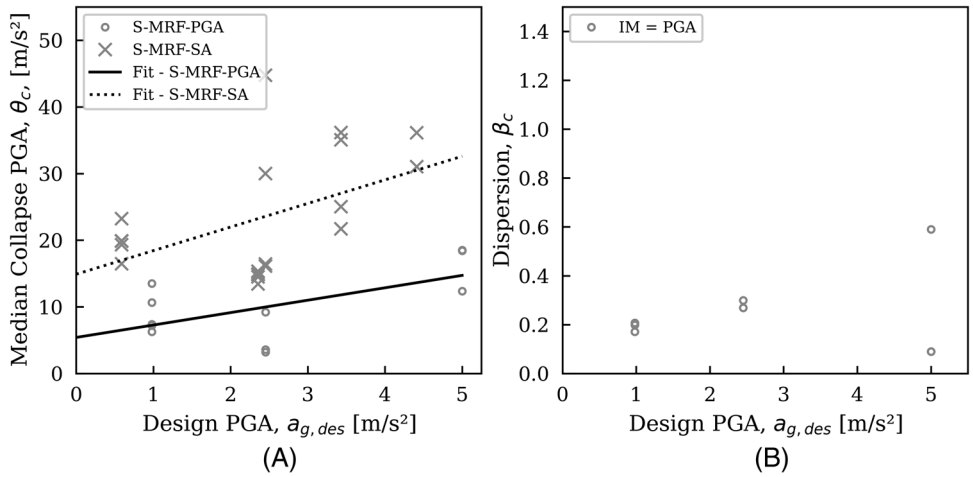

FIGURE 8 Steel fragility parameters from database. (A) θ_c and corresponding linear regression. (B) β_c.

given that the median collapse capacity appears to reduce for $a_{g,des} = 2.5\ m \cdot s^{-2}$ compared to $a_{g,des} = 1.0\ m \cdot s^{-2}$. However, the fit was performed to illustrate what is currently possible given the available data in the literature. The dispersion of the fragilities curves for the steel structures was assumed independent of $a_{g,des}$ because the small number of points available, and their obvious variation for large design PGAs, makes fitting unreliable. The constant dispersion was assumed equal to the mean of the points in Figure 8B and is presented in Table 2. As for the case of the RC structures, only the dispersions of derived from the fragility curves originally conditioned on PGA were considered.

2.7 | Additional sources of uncertainty

In §2.5 and §2.6, expressions were developed to describe the relationship between θ_c and $a_{g,des}$, and β_c and $a_{g,des}$; however, these expressions only predict the value of θ_c and β_c in a mean sense. Each of these parameters is associated with a certain level of dispersion about the mean value, as evidenced in Figure 5 to 8. This dispersion represents the variation in the response arising from models with different geometries and/or variations in the material parameters within a building typology, otherwise known as "modelling uncertainty". The consideration of the additional modeling uncertainty is an important aspect of the calculation of λ_c.

FEMA P695[15] proposed a model to account for modelling uncertainty based on the multiplicative combination of a series of independent lognormal random variables with a median value of unity and different dispersion values. Based on the FEMA P695 model, the total dispersion considered in the present study, β_{tot}, can be calculated using the equation,

$$\beta_{tot} = \sqrt{\beta_c^2 + \beta_\beta^2} \tag{6}$$

where β_c is the appropriate mean value of the dispersion as determined in the preceding sections and β_β is the modelling uncertainty. The values of β_β for each structural typology were determined by calculating the unbiased standard deviation of the dispersion values (e.g., the data points in Figure 7B) about the corresponding mean value (e.g., the black regression line in Figure 7B). The corresponding values of β_β are presented in the Table 2. Despite the small number of data points available for several of the typologies (e.g., S-MRF and RC-WDS), values of β_β were calculated for each structural typology; however, it is recommended that these values be verified with additional analysis results before being generalized.

The modelling uncertainty associated with the variation of θ_c about the mean value has not been considered in the calculation of β_{tot} because it is not lognormally distributed and cannot be combined with the other sources of uncertainty in this simplified manner.

Estimation uncertainty, also known as sample uncertainty, arises from the use of a finite number of data points to fit a particular regression model and the results in this study could be impacted by estimation uncertainty in the several ways. First, there is estimation uncertainty that comes with the values of the median collapse capacity and the corresponding dispersions taken from the literature.[46] This uncertainty is unfortunately difficult to quantify without the access to the

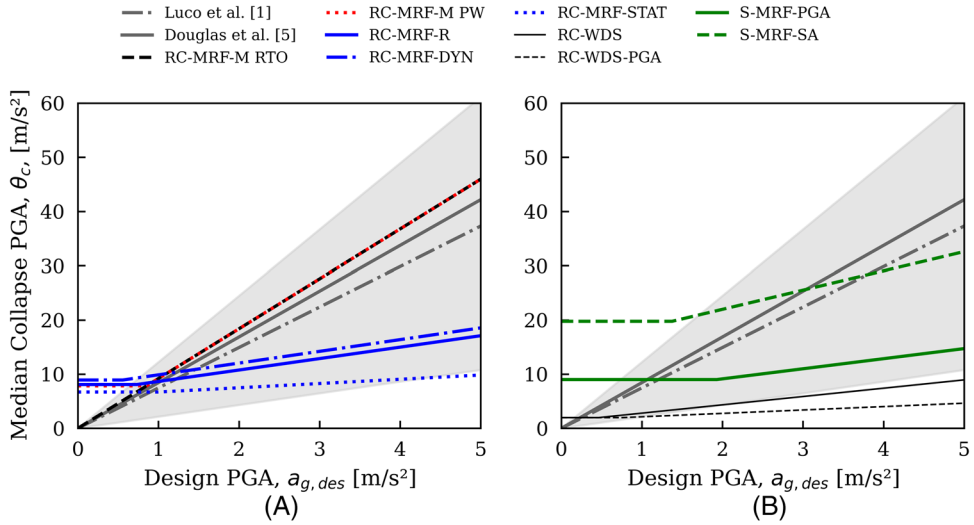

FIGURE 9 Comparison of the $\mathbf{a_{g,des} - \theta_c}$ relationship between the typology-specific fragility functions and functions from the literature. (A) functions for the RC-MRF-R and RC-MRF-M databases. (B) functions for the RC-WDS and S-MRF databases. M, medium; MRFs, moment-resisting frames; RC, reinforced concrete

detailed analysis underlying the fragility curves, however its consideration would certainly increase the dispersion of the data points around the lines of best fit derived herein. The second form of estimation uncertainty arises from the fitting of the $a_{g,des} - \theta_c$ relationships and the estimates of m_{θ_c} and c_{θ_c}. The variation of these parameters could be determined using bootstrapping methods; however, this was considered out of the scope of this study.

2.8 | Comparison of fragility functions

Figure 9 shows a comparison between the $a_{g,des} - \theta_c$ relationships derived in the preceding sections and several generic functions adopted from the literature. Most previous studies reviewed have not incorporated the inherent capacity of structures into their fragility curve formulation and assume that θ_c varies proportionally with $a_{g,des}$. Examples of the proportional relationships used by Douglas et al.[5] and Luco et al.[1] are included in Table 2 and Figure 9. The grey shaded area in the figure represents the maximum extent of the different $a_{g,des} - \theta_c$ relationships implied by the generic fragility curves reviewed in §1. It is worth noting here, that the fragility curve from Luco et al.[1] had to be modified so that it could be represented using a 475-year RTP design ground motion. To convert the original $P[C|\ a_g = a_{g,des}]$ of 10% for 2475-year RTP to an equivalent $P[C|\ a_g = a_{g,des}]$ for a 475-year RTP the procedure described by Silva et al.[10] was adopted, using only the hazard curves for Germany. The equivalent $P[C|\ a_g = a_{g,des}]$ for the 475-year RTP is 0.006. If a different set of hazard curves was used, then a different $P[C|\ a_g = a_{g,des}]$ would be obtained.[10] As it stands, this conversion is applicable in low seismicity regions in Europe, and specifically Germany.

It is immediately, obvious from Figure 9 that the slope of the expressions for RC-MRF-R, RC-WDS, and S-MRF are much shallower than the values from the literature. In contrast, the slope of the RC-MRF-M models agrees quite well with the generic curves. The inherent capacities (non-zero collapse capacity when $a_{g,des}$ is 0 m·s^{-2}) of the typology-specific fragility functions are also evident. The magnitudes of the inherent capacities are indicated in Table 2 and vary between 1.98 for the RC-WDS and 19.7 for the S-MRF-SA model. The inherent capacities of the RC-MRF lie between 6.7 and 8.9. The lines for RC-WDS lie completely outside the range of fragility functions proposed in the literature (Figure 9B). This indicates that the fragility curves used in previous studies may not be suitable for use in the design of wall structures. A long inherent capacity plateau is evident for the S-MRF-PGA model (Figure 9B), which can be attributed to the shallow slope of the best fit line.

Up until an $a_{g,des}$ of approximately 0.9 m·s^{-2}, the typology-specific models, except for RC-WDS, exhibit a higher median collapse capacity than the models from the literature. This reverses for values of $a_{g,des}$ above 0.9 m·s^{-2}. Subsequently, the median capacity of the typology-specific curves tends to be lower. For low values of $a_{g,des}$, the typology-specific curves imply less fragile structures compared to the generic functions, which is illustrated in Figure 10A for an $a_{g,des}$ of 0.5 m·s^{-2}.

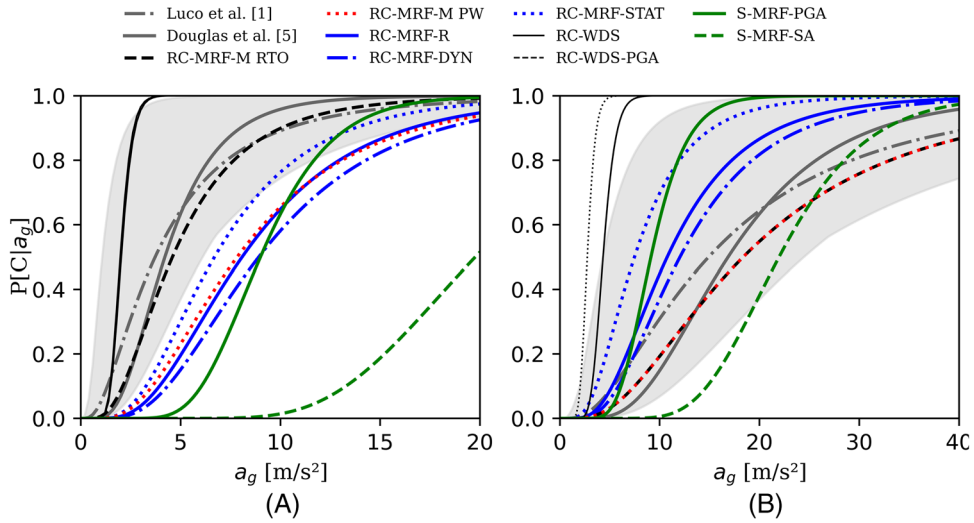

FIGURE 10 Comparison of the fragility functions for different design PGAs. (A)$\mathbf{a_{g,des}} = 0.5\ \mathrm{m{\cdot}s^{-2}}$ (B)$\mathbf{a_{g,des}} = 2.0\ \mathrm{m{\cdot}s^{-2}}$.

Each of the fragility curves was calculated using Equation (3) and the corresponding parameters from Table 2. Again, the grey area represents the maximum and minimum extents of the generic fragility curves reviewed in §1. At this intensity, it is easy to see the effect of the inherent capacity compared to the linearly proportional curves by observing that the RC-MRF-M PW curve lies much further to the right than the RC-MRF-M-RTO curve. In contrast, the curve for the more fragile RC-WDS lies to the extreme left of the figure.

It is interesting to note the similarities between the fragility curves of Luco et al.[1] and Douglas et al.[5] and the RC-MRF-M RTO model, which neglects the inherent capacity of the structures. From Figure 10A, the fragility function of Douglas et al.[5] appears to agree reasonably well with the RC-MRF-M RTO model for values of a_g around $a_{g,des}$. In contrast, the fragility curve of Luco et al.[1] appears to over predict the probability of collapse in this range when compared to the RC-MRF-M RTO model, implying that it may not be representative of European structures. However, for values of a_g larger than the 75th percentile there is good agreement between the fragility curve of Luco et al.[1] and the RCMRFM RTO model. As $a_{g,des}$ increases, the typology-specific fragility curves tend to move within the boundaries of the fragility models used in previous studies (Figure 10B). However, they represent structures that are more fragile than the curves of Luco et al.[1] and Douglas et al.[5] Here it can be seen that the RC-MRF-M-RTO and RC-MRF-M-PW curves are coincident, implying that the inherent capacity no longer governs the lateral capacity for the RC MRFs in this database. In contrast, the fragility curve for S-MRF-PGA remains unchanged due to the extremely long inherent capacity plateau previously identified.

In terms of dispersion, for an $a_{g,des}$ of $0.5\ \mathrm{m{\cdot}s^{-2}}$ the total dispersion, β_{tot}, is 0.61 for RC-MRF-M RTO and lies directly between the values of 0.5 and 0.8 adopted and Douglas et al.[5] and by Luco et al.,[1] respectively. This increase to approximately 0.7 for an $a_{g,des}$ of $2.0\ \mathrm{m{\cdot}s^{-2}}$.

3 | CALCULATION OF THE RISK-TARGETED REFERENCE PGA

As described previously, $a_{g,risk}$ for a particular site can be determined by solving the risk integral (Equation 1) iteratively. This is typically done using numerical integration, because the hazard curve resulting from a PSHA is not defined analytically. However, it possible to avoid the numerical integration by assuming that the hazard curve can be approximated as linear in log-log space using the following equation,[47]

$$H = k_o \left(a_g\right)^{-k_1} \tag{7}$$

where k_o and k_1 are the corresponding fitting coefficients. By applying this assumption to Equation (1) and assuming the typical lognormal collapse fragility function defined by θ_c and β_{tot}, a closed form expression for λ_c can be obtained,[47]

$$\lambda_c = k_0 \cdot \theta_c^{-k_1} \cdot e^{0.5k_1^2\beta_{tot}^2} \tag{8}$$

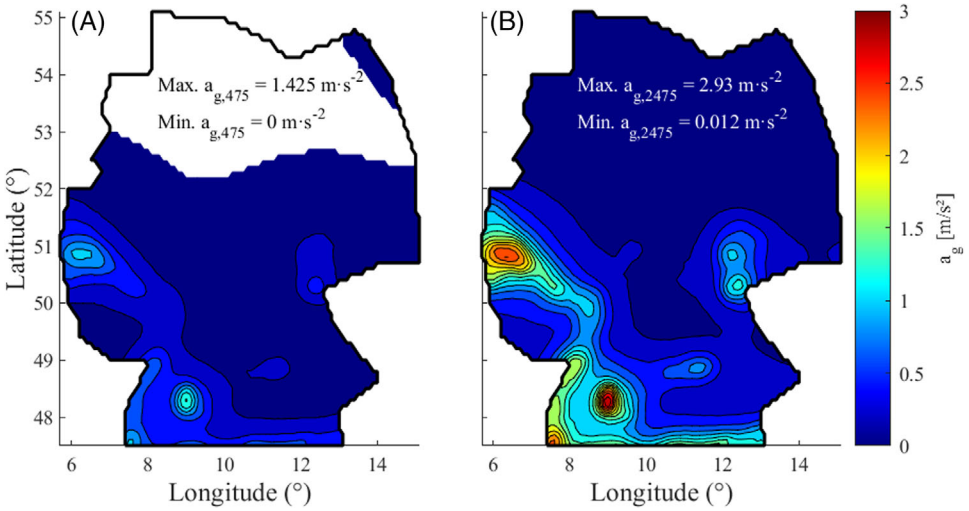

FIGURE 11 PGA hazard maps for Germany based on data from Grünthal et al.[49] (A) 475-year RTP, (B) 2475-year RTP.

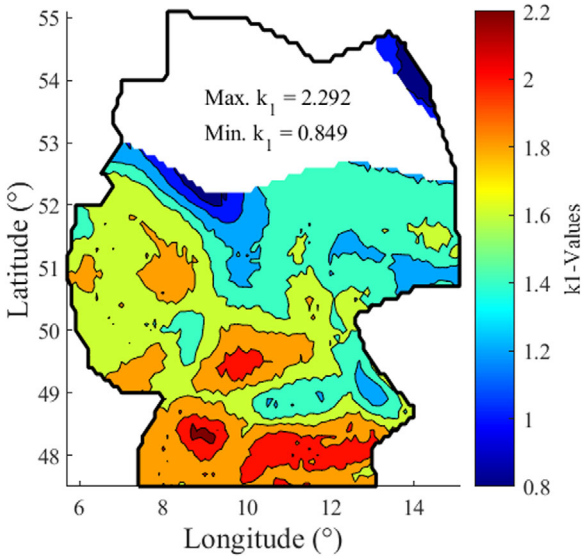

FIGURE 12 Spatial variation of the slope of the linearized hazard curve (k_1) across Germany.

Equation (5) was adopted in this study because the log-linear simplification of the hazard curve allows a solution for λ_c to be obtained when only a few points of the hazard curve are known. This is particularly useful in Germany, where the official hazard model is only tabulated for the 475-, 975-, and 2475-year RTPs.[45] For each site, the values of k_1 and k_0 were determined by fitting the log-linear hazard curve so that it passes through the points with RTPs of 475 and 2475 years, as proposed by Cornell.[47] This fitting procedure has been shown to produce results in close agreement with those obtained using the exact hazard curve and numerical integration.[48] Maps of the PGAs with RTPS of 475 and 2475 years are presented in Figure 11. The white regions on the maps have PGAs less than 0.01 m·s^{-2}, which was the minimum intensity in the provided dataset.[45] The spatial distribution of k_1 values, which represent the slope of the log-linear hazard curve, is presented in Figure 12.

The k_1 values presented in Figure 12 vary from 0.849 in the regions of lowest seismicity to up to 2.292 in the more seismically active areas. These values are significantly lower than three, which is quoted in Eurocode 8[3] as being a typical value for k_1. This indicates that in Germany the ratio of the intensities of less frequent ground motions (e.g., 2475-year RTP) to more frequent ground motions (e.g., 475-year RTP) is larger than suggested by Eurocode 8. This discrepancy has an impact on the assumed reliability of structures design according to Eurocode 8, particularly those with higher Importance classes, because it directly affects the relationship between the RTP and the importance factor (γ_I) which is defined in

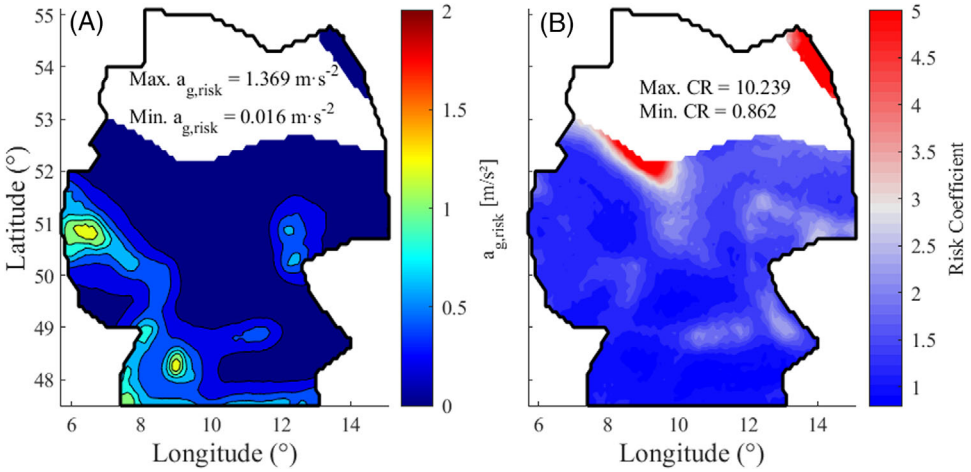

FIGURE 13 Risk-targeted seismic demands using the typology-specific fragility functions for RC-MRF-M RTO (A) $\mathbf{a_{g,risk}}$, (B) Risk coefficient—ratio $\mathbf{a_{g,risk}/a_{g,475}}$.

the Eurocode 8 as $\gamma_l = (\frac{T_{LR}}{T_L})^{-\frac{1}{k_1}}$, where T_{LR} is the reference RTP (usually 475 years) and T_L is the RTP of interest. When constant values of γ_l are adopted, as currently specified in the German national annex to Eurocode 8,[49] and k_1 varies as function of the location, the corresponding value of T_L must also vary. This indicates that the design RTPs for Importance Classes, other than the reference class, are not consistent across the country. Adopting a reliability-based approach, like the one in the present study, can help address this issue.

For calculating $a_{g,risk}$, in addition to defining the seismic hazard, a suitable value for the $\lambda_{c,t}$ must be chosen. Choosing a value of $\lambda_{c,t}$ can be difficult, as it is related to the level of risk that a community is willing to accept, which in turn, depends on many cultural, social, and economic factors. As a result, a variety of values are present in the literature. These tend to fall between 1×10^{-5} yr^{-1} and 5×10^{-4} yr^{-1}. A value of 2×10^{-4} yr^{-1} is currently proposed in the informative annex for reliability-based design verification in the draft version of the next generation of Eurocode 8.[50] It is worth noting that several studies suggest that this value may be too high when considering the impact of the loss of human life[10,14,51] and Douglas et al.[5] suggests that this would correspond to an unrealistically high average number of building collapses per annum if used in France. As a discussion around appropriate values of $\lambda_{c,t}$ is considered out of the scope of this study, a single value of $\lambda_t = 5 \cdot 10^{-5}$ was adopted for the derivation of the seismic demand maps. The adopted value is much stricter than that proposed by the Eurocode and is consistent with values derived based on casualty models.[10,14]

Each of the fragility curves discussed in §2.8 were used to determine $a_{g,risk}$, and the parameters for defining the corresponding $a_{g,des} - \theta_c$ can be found in Table 2. For each site, the iterative calculation was performed until the error between λ_c and $\lambda_{c,t}$ was less than 0.5% of $\lambda_{c,t}$.

4 | INFLUENCE OF FRAGILITY FUNCTIONS ON $a_{g,risk}$ MAPS FOR GERMANY

4.1 | Inherent lateral capacity

The $a_{g,risk}$ map, derived using the RC-MRF-M RTO fragility parameters, which does not account for the presence of the inherent lateral capacity, is presented in Figure 13A. The spatial distribution of the risk coefficient (CR) across Germany is shown in Figure 13B. The CR represents the ratio $a_{g,risk}/a_{g,475}$ and is useful for seeing if the design PGA needs to be increased (CR > 1.0) or reduced (CR < 1.0) to achieve the target reliability level.

Like the generic fragility functions proposed in the literature, the RC-MRF-M-RTO model assumes that the lateral capacity varies proportionally with $a_{g,des}$ and is independent of other factors that could influence the lateral capacity. A consequence of this proportionality assumption is that it is always possible to determine a value for $a_{g,risk}$ that produces a structure with the desired $\lambda_{c,t}$, even in regions with low seismicity such as central Germany (as evidenced by Figure 13), central France[5] or central Spain.[9] The spatial distribution of the probability of collapse in 50 years derived using the proportional RC-MRF-M RTO fragility model and the hazard-based 475-year RTP ground motions is presented in Figure 14A.

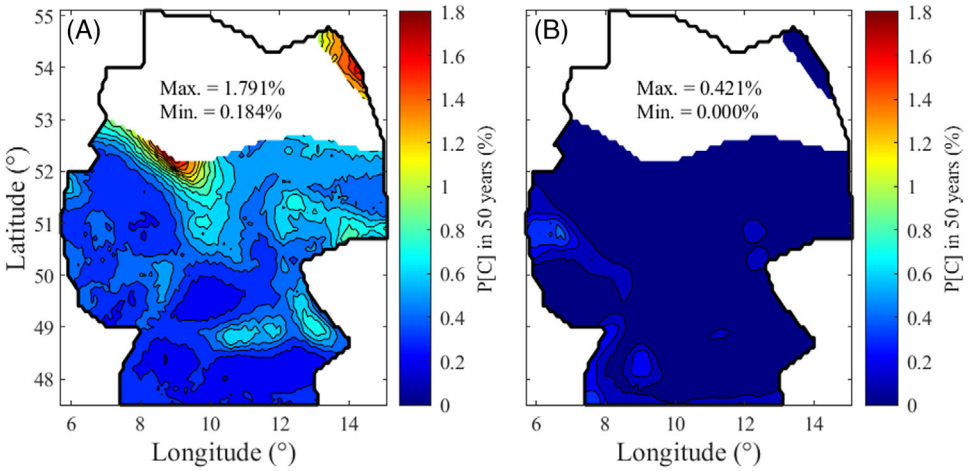

FIGURE 14 Probability of collapse in Germany implied by (A) the RC-MRF-M RTO fragility function (no inherent capacity); and (B) the RC-MRF-M-PW fragility function (includes inherent capacity). M, medium; MRFs, moment-resisting frames; piecewise model, PW; RC, reinforced concrete; RTO, regression through the origin.

This figure clearly shows that without using risk-targeting the collapse risk across Germany is not uniform. Additionally, the highest collapse rates occur in lowest seismic hazard regions. This is directly attributed to the use of the proportional fragility curve model.

When the inherent capacity is considered, it is not always possible to achieve the desired level of reliability in regions of low seismicity. This is because the inherent collapse capacity of the structure is greater than what is required to achieve the target reliability level, given the local hazard characteristics. To illustrate this point, if the fragility model RC-MRF-M PW (see §2.1.1, Table 2) is used in lieu of RC-MRF-M RTO in Equation (5), it is not possible to calculate values for $a_{g,risk}$ for all of Germany because the minimum lateral capacity (7.84 m·s^{-2}) results in λ_c values less than $\lambda_{c,t} = 5 \cdot 10^{-5}$ (0.25%) across large portions of country. As shown in Figure 14B, if the RC-MRF-M PW model is used, the maximum probability of collapse in 50 years was 0.421% ($\lambda_c = 8.42 \cdot 10^{-5}$)—just slightly larger than the target value. When attempting to derive maps using the typology-specific fragility functions for S-MRF-SA, S-MRF-PGA and RC-MRF-R databases suitable maps were unable to be derived because of the higher levels of inherent lateral capacity.

In contrast to the other typology specific fragility functions, it was possible to determine values of $a_{g,risk}$ for regions of Germany using the RC-WDS fragility function because of its low inherent capacity. However, due to a combination of this low inherent capacity and the low slope of $a_{g,des} - \theta_c$ relationship, the resulting $a_{g,risk}$ values were exceptionally large. The maximum calculated value of $a_{g,risk}$ was 14.693 m·s^{-2} which corresponded to a RTP of over 50,000 years.

4.2 | Comparison with existing fragility models

A comparison can be made between the $a_{g,risk}$ maps derived using the RC-MRF-M RTO parameters, and Figure 15 and Figure 16 which depict the $a_{g,risk}$ maps derived using the fragility curves of Douglas et al.[5] and Luco et al.,[1] respectively. Looking at Figure 13A, the maximum value of $a_{g,risk}$ is 1.369 m·s^{-2} and occurs in the southwestern corner of Germany, which corresponds to the area with the highest levels of seismic hazard (see Figure 11). The general form of the map is like the $a_{g,475}$ map, although note that the color scales are different. The values of CR vary between 0.862 and 10.239. Across most of Germany, CR varies between 1 and 2.5 indicating that an increase in the design acceleration above the 475-year RTP would be required to achieve the target risk level of 1×10^{-5}. The largest values of CR appear in the north of Germany in a few isolated locations that feature both the lowest $a_{g,475}$ values and the hazard curves with the shallowest slopes, whilst the lowest CR values generally occur in regions with higher PGA and steeper hazard curve slopes (see Figures 11 and 12). This observation, which is also evident in previous work,[10] is due to the slope of the linearized hazard curve, k_1. Flatter hazard curves (i.e., lower values of k_1) represent a more uniform distribution of hazard compared to steeper curves, which increases the influence that the higher intensity ground motions have on the mean annual frequency of collapse. This means that the collapse capacity (and therefore the design acceleration) needs to be increased to ensure the required

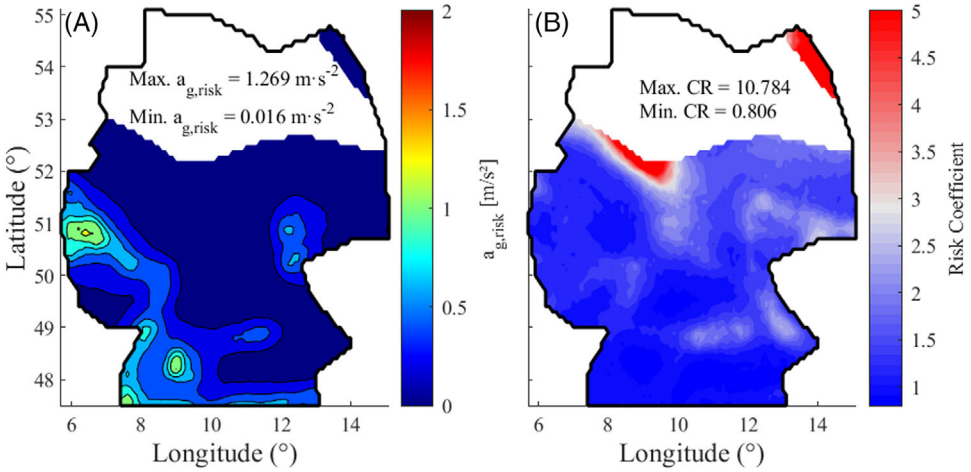

FIGURE 15 Risk-targeted seismic demands using the fragility function from Douglas et al.[5] (A) $\mathbf{a_{g,risk}}$, (B) Risk coefficient—ratio $\mathbf{a_{g,risk}/a_{g,475}}$.

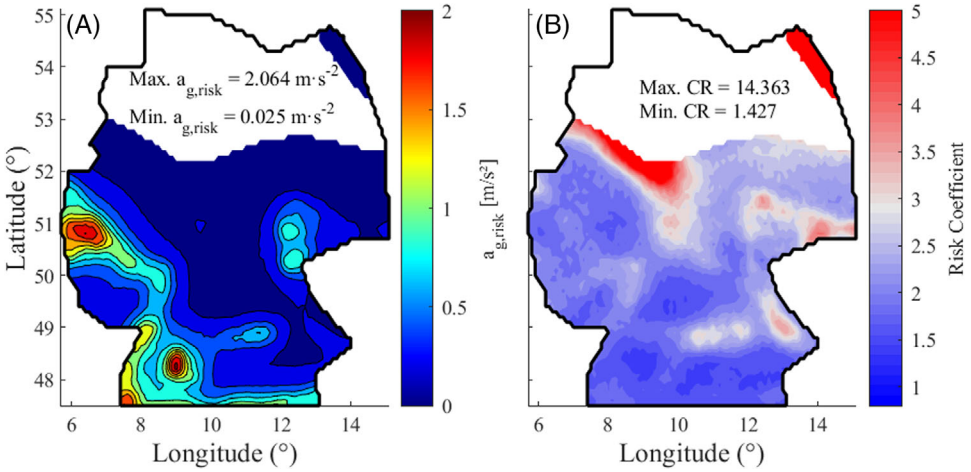

FIGURE 16 Risk-targeted seismic demands using the fragility function from Luco et al.[1] (A) $\mathbf{a_{g,risk}}$, (B) Risk coefficient—ratio $\mathbf{a_{g,risk}/a_{g,475}}$.

level of reliability. A brief visual comparison of Figures 13B and 12 tends to support that fact that CR is strongly influenced by the slope of the hazard curve as similar forms can be seen in the contours.

Comparing Figure 13 with Figures 15 and 16, it can be seen that the map derived using the fragility curve of Douglas et al.[5] (Figure 15) is in reasonably close agreement with the Figure 13, whereas the map derived using the fragility function of Luco et al[1] suggests higher values of $a_{g,risk}$. This can be attributed to the much higher $P[C|a_{g,des}]$ that was assigned to the fragility curve of Luco et al.,[1] as evidenced by Figure 9. Although the fragility curves for Luco et al.[1] and RC-MRF-M RTO are in good agreement above the 75th percentile, this has little effect on the $a_{g,risk}$ maps. This is because the ground motions that produce these high collapse probabilities also have a low MAFE, which reduces their influence on the calculation of λ_c. The fact that the PGA values in Figure 16 are up to 52% larger than those in Figure 13 indicates that the fragility curves proposed by Luco et al.[1] are not representative for European RC MRFs.

4.3 | Definition of seismic design regions

As previously discussed, the inherent collapse capacity is larger than the collapse capacity obtained from a purely proportional $a_{g,des} - \theta_c$ relationship for values of $a_{g,des}$ up to approximately 0.85–1.0 m·s^2. The fact that this inherent capacity is of a magnitude that results in acceptably low probabilities of collapse in low seismicity regions (Figure 14) suggests

the possibility of revising the areas where seismic design is required. Currently Eurocode 8 suggests that seismic design need not be considered for sites where $a_{g,475}$ is less than 0.5 m·s^{-2}[3]. Instead, regions requiring seismic design could be defined as any location where a structure with a pre-defined inherent capacity does not have the required level of collapse reliability. This definition could have a significant impact on the design of structures in regions of low seismicity, like Germany, where it is clear from Figure 14 that seismic design could be neglected. This discussion so far is predicated on the fact that the structures being designed are normal structures. If a structure of higher importance (implying a higher level of collapse reliability) is to be designed, then the inherent capacity may no longer be sufficient to ensure adequate performance and the regions where seismic design should be considered will have to be re-evaluated using an appropriate $\lambda_{c,t}$. Thus, the area where seismic design is compulsory is a function of the desired reliability level of the structures.

5 | RECOMMENDATIONS FOR FUTURE WORK

The most significant uncertainty highlighted by this work is the appropriate definition of typology-specific fragility curves for structures designed for different levels of design acceleration. It was illustrated how difficult it can be to find collapse fragility curves in the literature that represent new structures designed according to Eurocode 8 and along with sufficient information to characterize a relationship between the design acceleration and the median collapse capacity. This was particularly true for steel MRFs and RC WDS. Even for the most investigated structural typology, RC MRFs, there were only nine studies and a total of 136 fragility curves that were suitable for use. Within this set of fragility curves, the systematic difference between studies was significant enough that considering the curves as a single dataset could not be justified. To improve the reliability of risk-targeted seismic demand maps, it is recommended that extensive analysis campaigns, like the one conducted by Martins et al.,[16] be carried out to better characterize the typology-specific fragility curves. This work would go some way towards addressing some of the anomalies identified in this study, particularly the very low median collapse capacities observed in the S-MRF-PGA and RC-WDS databases. Examples of structural typologies requiring a significant increase in suitable collapse fragility data are steel MRFs; steel concentrically and eccentrically braced frames; RC WDS; brick masonry; and engineered timber MRFs and shear wall structures, amongst others. Before the extensive analysis begins it would be worthwhile defining a common framework for the development of the fragility curves (e.g., analysis methods, collapse definitions, modeling procedures, IMs etc.) to ensure consistency and compatibility across different studies. This would also make it much easier to harmonize the fragility data and incorporate it into a consistent set of expressions that can be adopted for the derivation of risk-targeted seismic demands for design standards and technical norms. A good starting point for development of such a framework could be the FEMA P695 report[15] and the SYNER-G project.[18]

The choice of the conditioning IM is also an important factor that should be considered in future research. With the SA of the response spectrum plateau and SA(T1 = 1s) replacing PGA as the anchors for the response spectrum, it would be worthwhile for future studies to develop fragility curves using one or both IMs. Additionally, the development of fragility curves using AvgSA would also be a valuable contribution to the development of risk-targeted seismic demand maps.

This study also highlights the effect that consideration of the inherent lateral capacity of structures can have on the development of $a_{g,risk}$ maps in low seismicity regions, namely, Germany. An appropriate characterization of the lateral capacity of structures designed for various magnitudes of wind, snow, and gravity loading, but neglecting seismic actions could be a useful tool for defining the extent of areas where seismic design is compulsory.

Expanding the number of typology-specific fragility functions to encompass more structural typologies and geometrical variations would result in a direct increase in the number of the seismic-maps, or tables of data that need to be published for a given territory. This can be seen as a drawback, given that many different maps and data tables would quickly become cumbersome for engineering practitioners to use. Several modifications to the risk-targeting method employed in this paper could overcome this potential issue. First, the risk-targeted seismic map could be created using a reference fragility curve and instead of the presenting the design PGA, it could show the median collapse PGA required to achieve the desired mean annual frequency of collapse. Then, the reference median collapse PGA could be modified using a simple equation derived from the simplified risk integral (Equation 8) to account for the difference in dispersion of the different structural typologies. Finally, the expressions for the median of typology-specific fragility curves (Table 2) could be used to obtain a type of reliability-based reduction factor that relates the median collapse PGA to the design PGA.

This study has been limited to Germany, which is characterized by relatively low seismic hazard, particularly when compared to other European countries like Italy, Greece, or Turkey. It would be beneficial if future research expanded this work and used typology-specific fragility functions produce risk-targeted seismic demand maps for higher seismicity

regions and investigate whether the key findings remain valid. Furthermore, designing a suite of structures and performing detailed collapse risk assessments could aim to verify that the typology-specific fragility curves employed in this study will produce a building stock with a more harmonized level of reliability.

6 | CONCLUSIONS

This study presented a preliminary investigation into the development and use of typology-specific fragility functions to derive risk-targeted PGA maps in regions of low seismicity. Expressions defining typology-specific fragility curves for RC MRFs, RC wall and dual systems, and steel MRFs were developed from a database of the fragility parameters collected from literature. These typology-specific fragility curves were used to investigate how the required design PGA varied between structural typologies if a uniform mean annual frequency of collapse was targeted. Variations in the fragility curve functions for the different structural typologies was observed, supporting the hypothesis that a single definition of the fragility curve as adopted in previous studies may not be suitable for ensuring uniform collapse risk. The resulting $a_{g,risk}$ maps were compared to several maps created using fragility relationships obtained from previous studies in the literature. It was found that the inherent capacity of structures designed without consideration of seismic loads had a significant influence on the maps. In regions of low seismicity, the inherent capacity may be sufficiently large to achieve the target reliability. The limitations and applications of this study were discussed in detail and recommendations were made for future research aimed at extending and verifying the results, particularly concerning the definition of the fragility curves.

ACKNOWLEDGMENTS

The authors would like to the acknowledge the valuable comments and remarks received from Dr Iunio Iervolino, Dr Vitor Silva, and an additional anonymous reviewer, that helped to greatly improve the quality of this manuscript.

Open access funding enabled and organized by Projekt DEAL.

CONFLICT OF INTEREST STATEMENT

The authors declare no conflicts of interest.

DATA AVAILABILITY STATEMENT

The data that supports the findings of this study and the MATLAB and Python scripts that have been used to conduct the analyses are openly available on our website: https://www.hsu-hh.de/stahlbau/en/earthquake-engineering.

REFERENCES

1. Luco N, Hamburger RO, Klemencic M, Seattle A, Jeffrey W, Kimball K. Risk-targeted versus current seismic design maps for the conterminous United States. Conference Proceedings SEAOC 2007, Squaw Creek: ASCE; 2007.
2. ASCE 7–10. *Minimum Design Loads for Buildings and Other Structures*. American Society of Civil Engineers; 2013. https://doi.org/10.1061/9780784412916
3. DIN. *Eurocode 8: Auslegung von Bauwerken gegen Erdbeben - Teil 1: Grundlagen, Erdbebeneinwirkungen und Regeln für Hochbauten, Deutsch Fassung EN 1998-1:2004 + AC:2009*. Berlin: DIN; 2010.
4. Jalayer F. Direct Probabilistic Seismic Analysis: Implementing Non-Linear Dynamic Assessments. *PhD Thesis*. Stanford: Stanford University; 2003.
5. Douglas J, Ulrich T, Negulescu C. Risk-targeted seismic design maps for mainland France. *Nat Hazards*. 2013;65(3):1999-2013. doi:10.1007/s11069-012-0460-6
6. Fiorini E, Bazzurro P, Silva V. Preliminary results of risk-targeted design maps for Italy. Second European Conference on Earthquake Engineering and Seismology. European Association for Earthquake Engineering (EAEE), Istanbul, Turkey, 2014.
7. Gkimprixis A, Tubaldi E, Douglas J. Derivation of risk-targeted maps for Italy based on a simplified approach. *XVIII Convegno Associazione Nazionale Italiana Di Ingegneria Sismica*. Pisa University Press, Pisa, Italy, 2019.
8. Vacareanu R, Pavel F, Craciun I, *et al.* Risk-targeted maps for Romania. *J Seismolog*. 2018;22(2):407-417. doi:10.1007/s10950-017-9713-x
9. Kharazian A, Molina S, Galiana-Merino JJ, Agea-Medina N. Risk-targeted hazard maps for Spain. *Bull Earthquake Eng*. 2021;19(13):5369-5389. doi:10.1007/s10518-021-01189-8
10. Silva V, Crowley H, Bazzurro P. Exploring risk-targeted hazard maps for Europe. *Earthquake Spectra*. 2016;32(2):1165-1186. doi:10.1193/112514EQS198M
11. Talebi M, Zare M, Noroozinejad Farsangi E, Soghrat MR, Maleki V, Esmaeili S. Development of risk-targeted seismic hazard maps for the Iranian plateau. *Soil Dyn Earthquake Eng*. 2021;141:106506. doi:10.1016/j.soildyn.2020.106506

12. Taherian AR, Kalantari A. Risk-targeted seismic design maps for Iran. *J Seismolog*. 2019;23(6):1299-1311. doi:10.1007/S10950-019-09867-6/TABLES/7
13. Pereira EMV, Cavalcante GHF, Andrade RB, Vieira Júnior LCM, Siqueira GH. Prospective study on risk-targeted seismic hazard maps for Northeastern Brazil: case study in Zone 1 of ABNT NBR 15421:2006. *Revista IBRACON de Estruturas e Materiais*. 2022;15(5). doi:10.1590/s1983-41952022000500005
14. Horspool N, Gerstenberger MC, Elwood KJ. Risk targeted hazard spectra for seismic design in New Zealand. *New Zealand Society for Earthquake Engineering Annual Conference*. New Zealand Society for Earthquake Engineering; 2021.
15. FEMA. *P695: Quantification of Building Seismic Performance Factors*. FEMA; 2009.
16. Martins L, Silva V, Bazzurro P, Marques M. Advances in the derivation of fragility functions for the development of risk-targeted hazard maps. *Eng Struct*. 2018;173:669-680. doi:10.1016/j.engstruct.2018.07.028
17. Crowley H, Silva V, Martins L. Seismic design code calibration based on individual and societal risk. 16th European Conference on Earthquake Engineering. June 18-21, 2018, Thessaloniki, Greece.
18. Pitilakis K, Crowley H, Kaynia AM. *Geotechnical, Geological and Earthquake Engineering SYNER-G: Typology Defi nition and Fragility Functions for Physical Elements at Seismic Risk Buildings, Lifelines, Transportation Networks and Critical Facilities*. 2014. doi:10.1007/978-94-007-7872-6
19. Ulrich T, Negulescu C, Douglas J. Fragility curves for risk-targeted seismic design maps. *Bull Earthquake Eng*. 2014;12(4):1479-1491. doi:10.1007/s10518-013-9572-y
20. Saruddin SNA, Nazri FM. Fragility curves for low- and mid-rise buildings in Malaysia. *Procedia Engineering*. 2015;125:873-878. doi:10.1016/J.PROENG.2015.11.056
21. Nazri FM, Tan CG, Saruddin SNA. Fragility curves of regular and irregular moment-resisting concrete and steel frames. *Int J Civ Eng*. 2018;16(8):917-927. doi:10.1007/S40999-017-0237-0/FIGURES/16
22. Gkimprixis A, Douglas J, Tubaldi E, Zonta D. Development of fragility curves for use in seismic risk targeting. 16th European Conference on Earthquake Engineering, June 18-21, 2018; Thessaloniki, Greece.
23. Lazar N, Dolšek M. Incorporating intensity bounds for assessing the seismic safety of structures: Does it matter? *Earthquake Eng Struct Dyn*. 2014;43(5):717-738. doi:10.1002/EQE.2368
24. Žižmond J, Dolšek M. Deaggregation of seismic safety in the design of reinforced concrete buildigs using Eurocode 8. 4th ECCOMAS Thematic Conference on Computational Methods in Structural Dynamics and Earthquake Engineering. June 12–14, 2013; Kos Island, Greece.
25. Kosič M, Dolšek M, Fajfar P. Dispersions for the pushover-based risk assessment of reinforced concrete frames and cantilever walls. *Earthquake Eng Struct Dyn*. 2016;45(13):2163-2183. doi:10.1002/eqe.2753
26. Aljawhari K, Gentile R, Freddi F, Galasso C. Effects of ground-motion sequences on fragility and vulnerability of case-study reinforced concrete frames. *Bull Earthquake Eng*. 2021;19(15):6329-6359. doi:10.1007/s10518-020-01006-8
27. Braconi A, Finetto M, Degee H, *et al. Optimising the Seismic Performance of Steel and Steel-Concrete Structures by Standardising Material Quality Control (OPUS)*. Publications Office; 2013. doi:10.2777/79330
28. Macedo L, Castro JM. Collapse performance assessment of steel moment frames designed to Eurocode 8. *Eng Fail Anal*. 2021;126:105445. doi:10.1016/j.engfailanal.2021.105445
29. Tartaglia R, D'Aniello M, Landolfo R. Seismic performance of Eurocode-compliant ductile steel MRFs. *Earthquake Eng Struct Dyn*. 2022;51(11):2527-2552. doi:10.1002/eqe.3672
30. DIN. *Eurocode 2: Bemessung and Konstruktion von Stahlbeton- und Spannbetontragwerken - Teil 1-1: Allgemeine Bemessungsregeln und Regeln für den Hochbau*. DIN; 2011.
31. DIN. *Eurocode 3: Bemessung und Konstruktion von Stahlbauten - Teil 1-1: Allgemeine Bemessungsregeln und Regeln für den Hochbau*. DIN; 2010.
32. Bravo-Haro MA, Elghazouli AY. Influence of earthquake duration on the response of steel moment frames. *Soil Dyn Earthquake Eng*. 2018;115:634-651. doi:10.1016/j.soildyn.2018.08.027
33. Gkimousis IA, Koumousis VK. Collapse fragility curves of RC Frames with varying design parameters. In: Papadrakakis M, Fragiadakis M, Plevris V, eds. *Computational Methods in Earthquake Engineering*, Vol. 2, Springer Science+Business Media; 2013.
34. Macedo L, Silva A, Castro JM. A more rational selection of the behaviour factor for seismic design according to Eurocode 8. *Eng Struct*. 2019;188:69-86. doi:10.1016/j.engstruct.2019.03.007
35. Antoniou K, Tsionis G, Fardis MN. Seismic fragility of concrete buildings. *4th International fib Congress*. fib; 2014.
36. Pnevmatikos NG, Papagiannopoulos GA, Papavasileiou GS. Fragility curves for mixed concrete/steel frames subjected to seismic excitation. *Soil Dyn Earthquake Eng*. 2019;116:709-713. doi:10.1016/j.soildyn.2018.09.037
37. Fardis MN, Papailia A, Tsionis G. Seismic fragility of RC framed and wall-frame buildings designed to the EN-Eurocodes. *Bull Earthq Eng*. 2012;10:1767-1793. doi:10.1007/s10518-012-9379-2
38. Papailia A, Tsionis G, Fardis MN. Effects of design to EN-eurocodes on the seismic fragility of concrete buildings. *15th World Conference on Earthquake Engineering*. Sociedade Portuguesa de Engenharia Sismica (SPES), Lisbon, Portugal 2012.
39. Hazus. *Hazus ®-MH 2.1 Technical Manual*. Hazus; 2012.
40. O'Reilly GJ. Limitations of Sa(T 1) as an intensity measure when assessing non-ductile infilled RC frame structures. *Bull Earthquake Eng*. 2021;19(6):2389-2417. doi:10.1007/s10518-021-01071-7

41. Kohrangi M, Bazzurro P, Vamvatsikos D, Spillatura A. Conditional spectrum-based ground motion record selection using average spectral acceleration. *Earthquake Eng Struct Dyn*. 2017;46(10):1667-1685. doi:10.1002/eqe.2876
42. Suzuki A, Iervolino I. Intensity measure conversion of fragility curves. *Earthquake Eng Struct Dyn*. 2020;49(6):607-629. doi:10.1002/EQE.3256
43. Baltzopoulos G, Grella A, Iervolino I. Seismic reliability implied by behavior-factor-based design. *Earthquake Eng Struct Dyn*. 2021;50(15):4076-4096. doi:10.1002/EQE.3546
44. Gündel M, Rapps C. Risikobasierte Erdbebenkarte für Deutschland. *16th D-A-CH Tagung Erdbebenenginieurwesen & Baudynamik*. Deutsche Gesellschaft für Erdbebeningenieurwesen und Baudynamic (DGEB), Kiel, Germany, Innsbruck, Austria 2019.
45. Grünthal G, Stromeyer D, Bosse C. *The Data Sets of the Earthquake Model for the Probabilistic Seismic Hazard Assessment of Germany, version 2016 - Technical Report STR17/05 - Data*. Potsdam; 2017. doi:10.2312/GFZ.b103-17056
46. Iervolino I. Estimation uncertainty for some common seismic fragility curve fitting methods. *Soil Dyn Earthquake Eng*. 2022;152:107068. doi:10.1016/J.SOILDYN.2021.107068
47. Cornell CA. Calculating building seismic performance reliability - a basis for multi-level design norms. *Eleventh World Conference on Earthquake Engineering*. Elsevier; 1996.
48. Gkimprixis A, Tubaldi E, Douglas J. Comparison of methods to develop risk-targeted seismic design maps. *Bull Earthquake Eng*. 2019;17(7):3727-3752. doi:10.1007/s10518-019-00629-w
49. DIN. *Nationaler Anhang-National festgelegte Parameter-Eurocode 8: Auslegung von Bauwerken gegen Erdbeben-Teil 1: Grundlagen, Erdbebeneinwirkungen und Regeln für Hochbauten, mit CD-ROM*. DIN; 2021.
50. CEN. *Draft EN1998-1-1_version_01-10-2021: Eurocode 8: Design of Structures for Earthquake Resistance-Part 1-1: General Rules and Seismic Action*. CEN; 2004.
51. JCSS. *Probabilistic Model Code Part 1: Basis of Design*. JCSS; 2001.
52. Grünthal G, Stromeyer D, Bosse C, Cotton F, Bindi D. The probabilistic seismic hazard assessment of Germany—version 2016, considering the range of epistemic uncertainties and aleatory variability. *Bull Earthquake Eng*. 2018;16(10):4339-4395. doi:10.1007/s10518-018-0315-y

How to cite this article: Clemett N, Rapps C, Gündel M. Evaluation of typology-specific fragility curves used for risk-targeted seismic demand maps in regions of low seismicity: A German case-study. *Earthquake Engng Struct Dyn*. 2023;1-22. https://doi.org/10.1002/eqe.3911